

1 Slowdown of Shirase Glacier, East Antarctica, caused by strengthening alongshore winds

2

3 Bertie W.J. Miles*^{1,2}, Chris R. Stokes², Adrian Jenkins³, Jim .R. Jordan^{3,4}, Stewart .S.R. Jamieson²,
4 G. Hilmar. Gudmundsson³

5

6 ¹School of Geosciences, Edinburgh University, Edinburgh, EH8 9XP, UK

7 ²Department of Geography, Durham University, Durham, DH1 3LE, UK

8 ³Department of Geography and Environmental Sciences, Northumbria University, Newcastle upon
9 Tyne, NE1 8ST, UK

10 ⁴Laboratoire de Glaciologie, Université Libre de Bruxelles, Brussels, Belgium

11 *Correspondence to Bertie.Miles@ed.ac.uk

12

13 Abstract

14 Around large parts of West Antarctica and in Wilkes Land, East Antarctica, increased wind-forced
15 intrusions of modified Circumpolar Deep Water (mCDW) onto the continental shelf have been
16 associated with mass loss over the last few decades. Despite considerable seasonal variability,
17 observations in 2018 have also confirmed relatively high basal melt rates of up to 16 m a⁻¹ underneath
18 the Shirase ice tongue in Enderby Land, East Antarctica. These high basal melt rates are also caused
19 by intrusions of mCDW onto the continental shelf, but the catchment of Shirase Glacier has been
20 gaining mass, a trend often attributed to increased precipitation. Here, we document the dynamical
21 ocean-driven slowdown, ice surface thickening and grounding line advance of Shirase Glacier, in
22 response to strengthening easterly winds that reduce mCDW inflow and decrease basal melt rates.
23 Our findings are significant because they demonstrate that warm ice shelf cavity regimes are not
24 universally associated with glacier acceleration and mass loss in Antarctica, and they highlight the
25 overlooked role of the impact of easterly winds in the recent mass gain of the Shirase Glacier
26 catchment.

27

28 1. Introduction

29 Shirase Glacier is one of the fastest flowing outlet glaciers in East Antarctica, reaching speeds in
30 excess of $2,200 \text{ m a}^{-1}$ across its grounding line, before flowing into Lützow-Holm Bay (Fig. 1). Its
31 annual ice discharge approaches 15 Gt a^{-1} (Rignot et al., 2019) and it drains a catchment containing
32 1.2 m of sea level equivalent (Fig.1, Morlighem et al., 2020). This rapid ice flow speed is associated
33 with vigorous melt underneath its floating tongue, where basal melt rates were observed to vary over
34 the course of the year between 7 and 16 m a^{-1} in 2018, 16 km downstream of the glacier's grounding
35 line (Hirano et al., 2020). These high melt rates are caused by warm modified Circumpolar Deep
36 Water (mCDW) intruding onto the continental shelf and being transported directly to the glacier via
37 bathymetric troughs (Fig. 1; Moriwaki & Yoshida, 1983; Hirano et al., 2020), a process referred to
38 as Mode 2 melting (Jacobs et al., 1992). Elsewhere in Antarctica, most regions that experience this
39 mode of oceanic melt have been losing mass e.g. the Amundsen Sea (Jenkins et al., 2018; Mougnot
40 et al., 2014), the Western Antarctic Peninsula (Cook et al., 2016) and Wilkes Land (Rintoul et al.,
41 2016; Greene et al., 2017; Stokes et al., 2022); and hinting that intrusions of mCDW have become
42 more potent over recent decades in these locations. However, mass loss has not been observed in the
43 Shirase Glacier catchment and, between 2003 and 2019, its drainage basin (sometimes referred to as
44 drainage basin 7 in Antarctic-wide studies (e.g. Smith et al., 2020) gained mass at a rate of $+25 \pm 6$
45 Gt a^{-1} , which is the largest magnitude of imbalance of all drainage basins in East Antarctica (Smith
46 et al., 2020), including the comparatively well studied drainage basin 13 in Wilkes Land ($-20 \pm 14 \text{ Gt}$
47 a^{-1}).

48 The mass gain and thickening in the Shirase catchment over the past two decades (Schröder et al.,
49 2019; Smith et al., 2020) has been hypothesized to have been caused by increased precipitation across
50 the wider Dronning Maud and Enderby Land regions (Smith et al., 2020). Prior to this, however,
51 earlier field-based estimates, using repeat triangulation surveys in 1969 and 1973, demonstrated ice
52 surface lowering of around 0.7 m a^{-1} around $100\text{-}200 \text{ km}$ inland of the Shirase Glacier grounding line
53 (Mae & Naruse, 1978; Naruse, 1979; Nishio et al., 1989). Furthermore, repeat GPS surveys in 1980
54 and 1988 revealed a thinning rate of around 0.5 m a^{-1} around $100\text{-}150 \text{ km}$ inland of the grounding
55 line (Toh et al., 1992). These rates of surface lowering during that time are comparable with some of
56 the fastest rates of thinning observed across Antarctica over the past decade and occurred at similar
57 distances inland of the grounding line (Smith et al., 2020). Moreover, this surface lowering in the
58 1970s and 1980s may have been part of a much longer-term signal with ice core records estimating
59 a surface lowering of 350 m over the past 2000 years of the Mizuho Plateau (Kameda et al., 1990),
60 which is located around 200 km inland of the Shirase coastline. The surface lowering over the past
61 2000 years is also coincident with an increase in ice discharge from the Lützow-Holm Bay, which
62 has been estimated from subglacial erosion rates (Sproson et al., 2021).

63 Oceanographic observations in Lützow-Holm Bay in 2018 have revealed a two-layered structure with
64 a cool and relatively fresh layer of Winter Water overlying a warm and saline layer of mCDW, where
65 temperatures near the ice front seasonally exceed the *in situ* melting point by 2.7 °C (Hirano et al.,
66 2020). Observations and modelling demonstrate a strong seasonal variation in the basal melt rate of
67 the Shirase ice tongue (Hirano et al., 2020; Kusahara et al., 2021), which is caused by seasonal
68 variations in the depth of the thermocline forced by the strength of the alongshore easterly winds near
69 the continental shelf (Ohshima et al., 1996). To date, there is no evidence of large seasonal variations
70 in ice flow speed at the grounding line, but observations show some seasonal variation in ice flow
71 speed on the floating tongue that could be connected to external forcing (Nakamura et al., 2007;
72 2010).

73 There have been several studies analysing the ice flow dynamics of the Shirase Glacier, largely
74 covering short sub-decadal time periods (Pattyn & Derauw, 2002; Pattyn & Naruse, 2003; Nakamura
75 et al., 2010; Aoyama et al., 2013). However, the longer-term geological signal of ice sheet thinning
76 and increased ice discharge (Sproson et al., 2021), along with observations of thinning in the 1970s
77 and 1980s (Mae & Naruse, 1978; Naruse, 1979; Nishio et al., 1989; Toh et al., 1992), followed by
78 thickening from the 2000s (Schröder et al., 2019; Smith et al., 2020) raise some important questions
79 into the processes causing this switch from mass loss to mass gain. In this study, we produce a time
80 series of ice flow speed that spans 47 years and show that long-term ice speed trends coincide with
81 alongshore wind speeds and their impact on intrusions of mCDW. We then discuss how these
82 observations may relate to wider hemispheric trends in atmospheric circulation and what this may
83 mean for the future mass balance of the Shirase catchment and the wider Dronning Maud and Enderby
84 Land sectors.

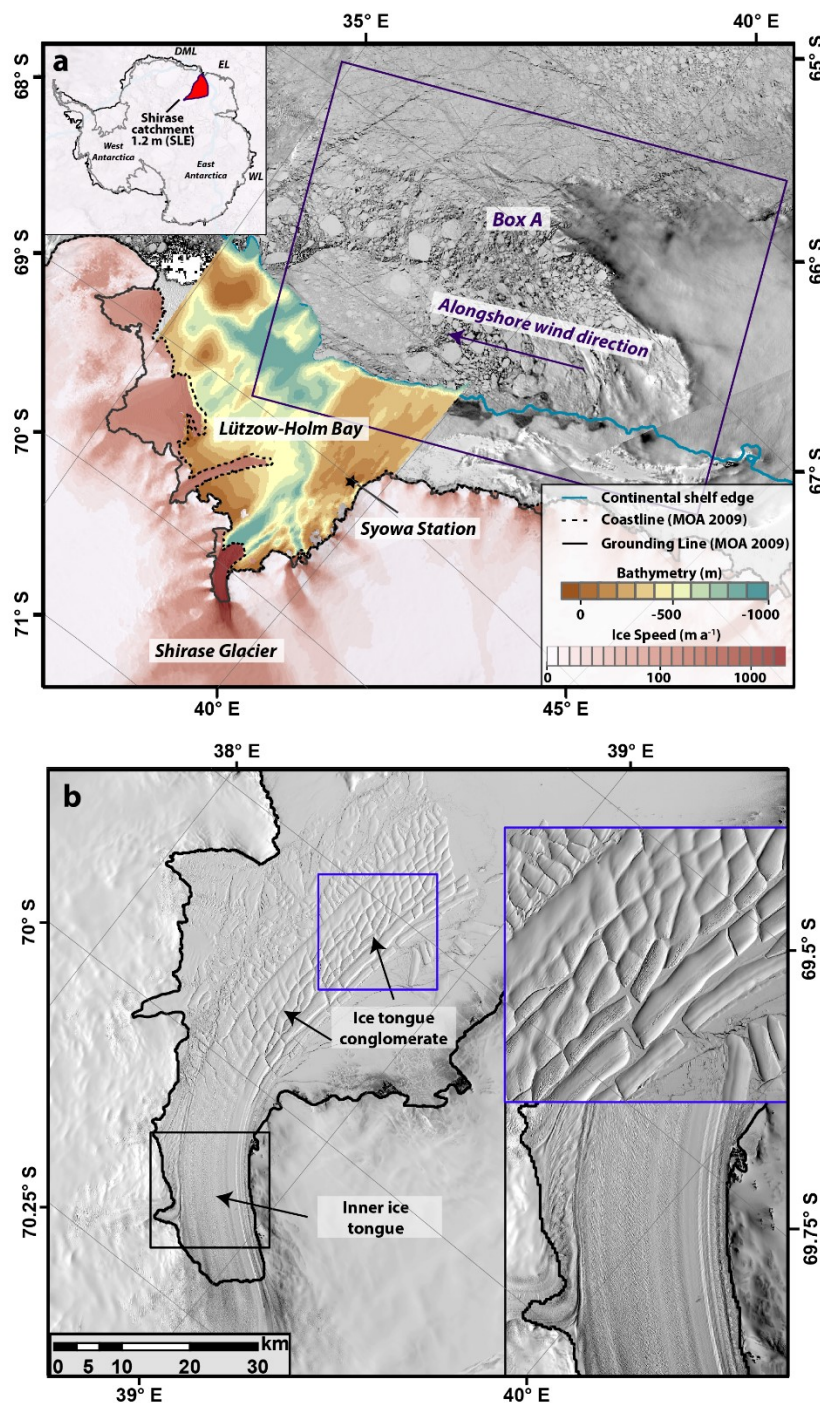
85

86 **2. Data and Methods**

87 **2.1 Ice-front position, ice speed, grounding line and ice thickness**

88 We create a time series of ice-front positions between 1963 and 2020 using a variety of different
89 sources including: ARGON imagery from 1963, Landsat-1 imagery from 1973, Landsat-5 imagery
90 from 1984, Landsat-4 imagery from 1988, RADARSAT RAMP mosaic from 1997 (Jezek et al.,
91 2013), and MODIS imagery from 2000-2020, with the spatial resolution of the satellite data ranging
92 from 15-250 m. In each case, we map the outer limit of the collection of loosely bound icebergs that
93 form the Shirase ice tongue that are typically surrounded by a smoother surface of fast ice (Fig. 1 &
94 2a). Errors associated with this mapping are insignificant in the context of the ice tongue typically
95 advancing 2,500 m a⁻¹, or retreating in short-lived calving events typically greater than 10 km.

96 We calculate 18 ice speed estimates for Shirase Glacier between 1973 and 2020. For 1973 we use a
 97 pair of Landsat-1 (band 7) images from the 25th January 1973 and the 21st January 1974 that we
 98 manually co-register to each other, before co-registering to a Landsat-8 image. The combination of
 99 the relatively coarse Landsat-1 imagery (60 m) and the development of surface melt ponding over the
 100 fast-flowing section of the glaciers between the two images prevented the automatic extraction of ice
 101 speed. Instead, we extract an ice speed estimate by manually tracking the displacement of a prominent
 102 rift ~24 km downstream of the grounding line (Fig. 2d). Errors associated with the manual tracking
 103 of this rift stem from the co-registration between the two image pairs which we estimate to be one



105 **Figure 1: a)** MODIS image of Lützow-Holm Bay and Shirase Glacier from the 4th November 2019
106 obtained from NASA WorldView. Overlain is the ITS_LIVE composite velocity product in
107 logarithmic scale (Gardner et al., 2018; 2020), 1000 m bathymetric contour obtained from
108 BedMachine (Morlighem et al., 2020) which is taken as the continental shelf boundary and
109 bathymetry of the Lützow-Holm Bay (Kusahara et al., 2021). Note the deep trough connecting Shirase
110 Glacier to the open ocean. The location of the Syowa research station and Box A, the region where
111 ERA5 derived winds were extracted are also shown. The initials in the inset refer to the following,
112 DML (Dronning Maud Land), EL (Enderby Land), WL (Wilkes Land). **b)** Landsat 8 image from
113 November 2020 showing the structure of the Shirase ice tongue. The blue box is a zoomed in section
114 of the ice tongue conglomerate that is unconstrained. The black box is a zoomed in section of the
115 inner section of the ice tongue that is constrained by fjord walls on either side. The black line on both
116 images is the MODIS 2009 grounding line and coastline (Scambos et al., 2007; Harran et al., 2019).
117 Landsat images are courtesy of the U.S. Geological Survey.

118

119 pixel (60 m; Animation S1). For 1988, we use a pair of Landsat-4 (band 3) images from the 14th
120 January 1988 and the 15th February 1988 that we also co-register to a Landsat-8 image. The quality
121 of the Landsat-5 images (30 m resolution) is superior to that of the Landsat-1 imagery and, in the
122 absence of significant surface melt ponding, we use the feature tracking software COSI-CORR
123 (Leprince et al., 2007; Scherler et al., 2008) to extract ice speed. For these images, co-registration
124 error is negligible (Animation S2) and error in the feature tracking is estimated at <0.5 pixels (e.g.
125 Heid and Kääb, 2012). Because of the close time separation of the image pairs this results in a larger
126 error of $\pm 171 \text{ m a}^{-1}$.

127 For 2000-2018 we use 14 annual ice speed mosaics from the ITS_LIVE dataset which cover Shirase
128 Glacier (Gardner et al., 2018) and use the corresponding error grids for error values, which range
129 from ± 1 to $\pm 32 \text{ m a}^{-1}$. For 2019 ($n = 27$) and 2020 ($n = 19$) we take an average of all GoLIVE generated
130 ice speed fields (Fahnestock et al., 2016; Scambos et al., 2016) with a time separation of 16-320 days
131 from scene ID's 149_109 and 150_109. Taking an average of multiple ice speed grids reduces error
132 and, as such, we prescribe a nominal error of 16 m a^{-1} , based on the average value from the ITS_LIVE
133 mosaics. We extract ice speed profiles from each time period across a transect, T1 (Fig. 2a), and also
134 produce a time-series of ice speed change where T1 crosses the grounding line. In 1973, the only
135 possible observation of ice speed was extracted 24 km downstream of the grounding line (Point x;
136 Fig. 2a) and there are no observations directly at the grounding line. To account for this, we estimate
137 ice speed at the grounding line in 1973 using the average difference between point x, 24 km
138 downstream of the grounding line, and where T1 crosses the grounding line in each of the other 17
139 ice speed profiles (1988-2020). Across these profiles, ice speed was on average 2% slower (ranging
140 from 1% to 4%) at the grounding line, compared to ice speed at point x. Therefore, to estimate ice
141 speed at the grounding line in 1973 we reduce the ice speed observed 24 km downstream of the

142 grounding line by $2 \pm 1\%$. We also include the measurements of ice speed from Nakamura et al. (2007)
143 at the grounding line derived from the JERS-1 satellite in 1996, 1997 and 1998.

144 To estimate the direction and magnitude of any migration in the Shirase Glacier grounding line we
145 compare time stamped digital elevation model (DEM) strips with a spatial resolution of 2 m from the
146 6th January 2013 and the 8th October 2015 from the REMA project (Howat et al., 2019). We select
147 these strips because they cover the complete Shirase Glacier grounding line and represent the longest
148 time gap in the record. This is in addition to a SPOT5-HRS DEM from the SPIRIT project (Korona
149 et al., 2009) from the 8th February 2008, with a spatial resolution of 40 m. Elevation uncertainty is
150 estimated at around 4 m by comparing derived elevations from exposed bedrock between the two
151 REMA DEM's and a larger uncertainty of around 7 m between the SPOT5-HRS and REMA DEM's.
152 The tidal amplitude of the region is limited to 0.2 m (Aoki et al., 2000) and is deemed insignificant.
153 We extract elevation profiles along transect T1 (Fig. 2a) from these dates. A comparison of elevation
154 profiles cannot provide a location of the true grounding line position, but any horizontal migration of
155 these elevation slopes can provide reasonable estimates in both the direction and rate of grounding
156 line migration (Fricker et al., 2009; Brunt et al., 2010).

157 We also extract an ice thickness change time-series from the dataset presented in Schröder et al.
158 (2019) from point IT, which is around 20 km inland of the grounding line (Fig. 2a). This multi-
159 mission dataset spans between 1978 and 2017 and contains data from a variety of satellites. We use
160 the accompanying uncertainty estimates described in Schröder et al. (2019). We also utilize modelled
161 basal melt rate anomalies of the Shirase ice tongue that are derived by an ocean model that is forced
162 by ERA-Interim wind reanalysis between 2008 and 2018 by Kusahara et al. (2021). The basal melt
163 rate dataset contains melt anomalies that have been simulated with fast ice cover and a hypothetical
164 no fast ice scenario (see Fig. 20; Kusahara et al., 2021). We use the melt rates with fast ice cover
165 because persistent fast ice cover remained throughout our observational period, aside from a few
166 sporadic partial breakouts in the summer months.

167

168 **2.2 Climatological data**

169 We extract mean monthly ERA5 (Hersbach et al., 2020) 10 m zonal (U) and meridional winds (V)
170 speeds with a gridded 30 km spatial resolution between 1979 and 2021 from a box approximately
171 340 x 250 km adjacent to the coastline (Box A; Fig. 1a). We do not extend the box all the way into
172 Lützow-Holm Bay because it is semi-permanently covered with landfast sea-ice (Fig. S1) that
173 dampens the impact of winds on ocean circulation. We then calculate alongshore easterly wind speed
174 using an alongshore angle of 80° from due north:

175

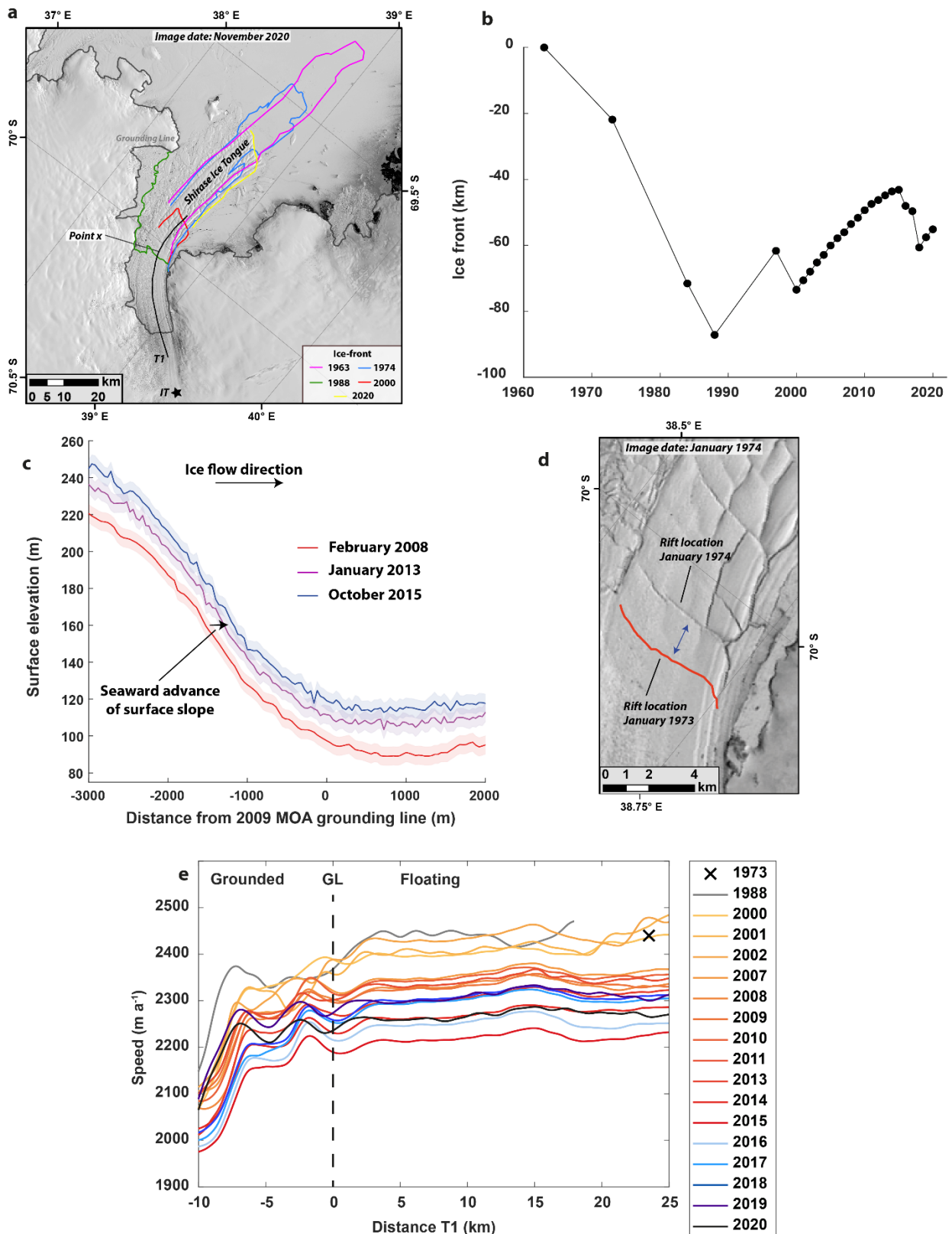
$$A = W \cos(\theta - 80)$$

176 Where W is wind speed and θ is wind direction. Using the ERA5 data, we also calculate the linear
177 trend in zonal wind between 1979 and 2021 across a wider region of the Dronning Maud and Enderby
178 Land coastlines. We also extract a precipitation time series across Shirase Glacier using the regional
179 climate model MAR between 1979 and 2019 (Kittel et al., 2021).

180

181 **3. Results**

182 We observe a total range of nearly 90 km in the ice-front position of the Shirase ice tongue between
183 1963 and 2020 (Fig. 2a, b). Its maximum length was in 1963, before retreating to its minimum extent
184 in 1988 (Fig. 2a, b). Since 1988 there has been a general pattern of advance with a few sporadic
185 calving events (Fig. 2a, b). Most of the variation in the extent of the Shirase ice tongue is in the
186 heavily fractured and unconstrained ice tongue conglomerate (Fig. 1b; Fig. 2a). The only exception
187 to this was in 1988 when the ice tongue retreated to the entrance of the narrow and more constrained
188 section of its fjord, 24 km advanced of its 2009 grounding line (Fig. 2a).



189

190 **Figure 2:** a) Landsat-8 image from November 2020 showing the Shirase ice tongue. Overlain are
 191 selected ice-front positions from 1963, 1974, 1988, 2000 and 2020; along with the transect, T1, used
 192 to extract ice speed profiles and point x, which is the location of the 1973/74 ice speed estimate on
 193 the floating tongue. Point IT is the location of the ice thickness time-series. The grey line is the
 194 MODIS 2009 grounding line (Scambos et al., 2007, Harran et al., 2021). b) Change in ice-front extent

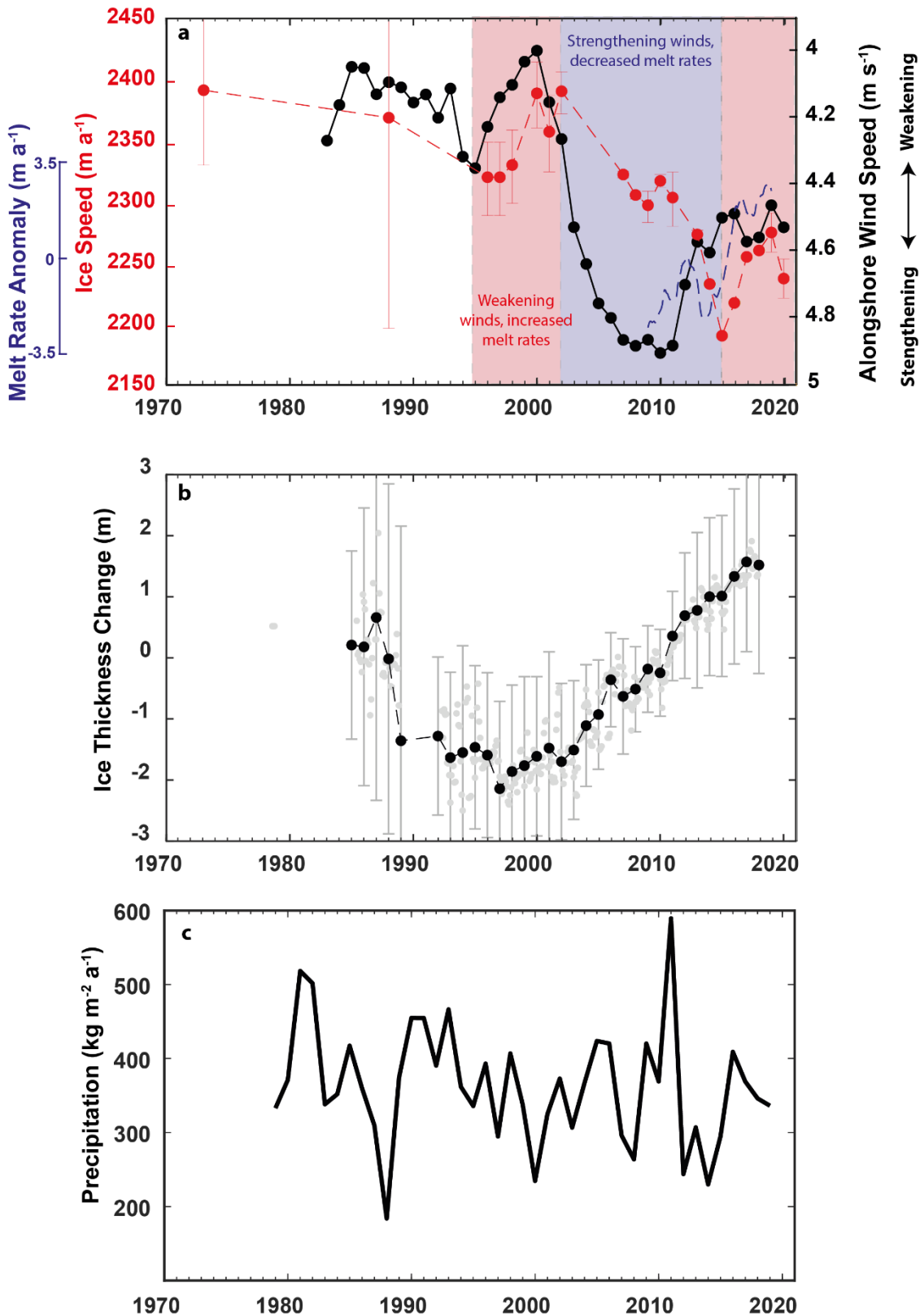
195 relative to 1963. **c)** Surface elevation profiles along a small section of T1 as it intersects the grounding
196 line from February 2008, January 2013 and October 2015 showing a seaward migration of the surface
197 slope **d)** Landsat-1 image showing the rift used to estimate ice speed in 1973/74. The red line is the
198 digitized rift from January 1973. **e)** Ice speed profiles from transect T1 between 1973 and 2020. The
199 black cross represents the ice speed measurement from 1973/74. Landsat images are courtesy of the
200 U.S. Geological Survey.

201

202 Ice speed profiles along the transect (T1, Fig. 2a) show a uniform pattern of change across both the
203 grounded and floating sections of Shirase Glacier (Fig. 2e). At the grounding line, we observe little
204 change in ice speed between 1973 and 1988, although we note the larger uncertainty in the 1988
205 estimate of $\pm 171 \text{ m a}^{-1}$ (Fig. 3a) and we cannot rule out interannual variations in ice speed within this
206 date range. Between 1988 and 1996 we observe a $2 \pm 7\%$ slowdown and a $2 \pm 1\%$ increase in ice speed
207 between 1997 and 2000 (Fig. 3a). Post-2000 we observe a slowdown, with an $8 \pm 1\%$ decrease in ice
208 speed between 2000 and 2015 (Fig. 3a). Between 2015 and 2019 ice speed increased by $4 \pm 1\%$ (Fig.
209 3a). Observations of ice thickness change 20 km inland of the grounding line show a thinning trend
210 of $0.27 \pm 0.33 \text{ m a}^{-1}$ between 1987 and 1997, before reversing to a thickening trend of $0.19 \pm 0.10 \text{ m}$
211 a^{-1} between 1997 and 2017 (Fig. 3b). There is large interannual variability in precipitation over
212 Shirase Glacier (Fig. 3c) and no obvious link to observations in ice speed or ice thickness. Elevation
213 profiles along a section of T1 in 2008, 2013 and 2015 show a consistent seaward migration of the
214 surface slope as it approaches the grounding line (Fig. 2c, animation S3). The absence of any
215 consistent increases in precipitation suggests that this is predominantly a horizontal offset caused by
216 grounding line advance. Therefore, between February 2008 and October 2015 we estimate that the
217 grounding line advanced around 400 m ($\sim 50 \text{ m yr}^{-1}$) from measuring the seaward displacement of the
218 surface slope, an estimate that is broadly consistent with CryoSat based observations of seaward
219 grounding line migration between 2010 and 2016 ($\sim 30 \text{ m a}^{-1}$; Konrad et al., 2018).

220 ERA5 derived estimates of alongshore easterly wind speed between 1979 and 2020 show limited
221 variation between 1984 and the early 1990s (Fig. 3a). In the early 1990s there was a small increase
222 in alongshore wind speed, before a more marked increase from 2000-2010 where alongshore wind
223 speed increased from around 4 m s^{-1} to 4.8 m s^{-1} (Fig. 3a). This is before falling slightly to around 4.5
224 m s^{-1} between 2010 and 2018, which is coincident with an increase in basal melt rate anomalies (Fig.
225 3a). The multidecadal trend in zonal wind shows a trend for a strengthening of wind in an easterly
226 direction at the continental shelf boundary over much of Enderby Land (Fig. 4). There is no trend in
227 zonal wind speed over large parts of Dronning Maud Land, with the exception of near Jutulstraumen
228 Glacier where there is a trend for strengthening wind in the westerly direction (Fig. 4).

229

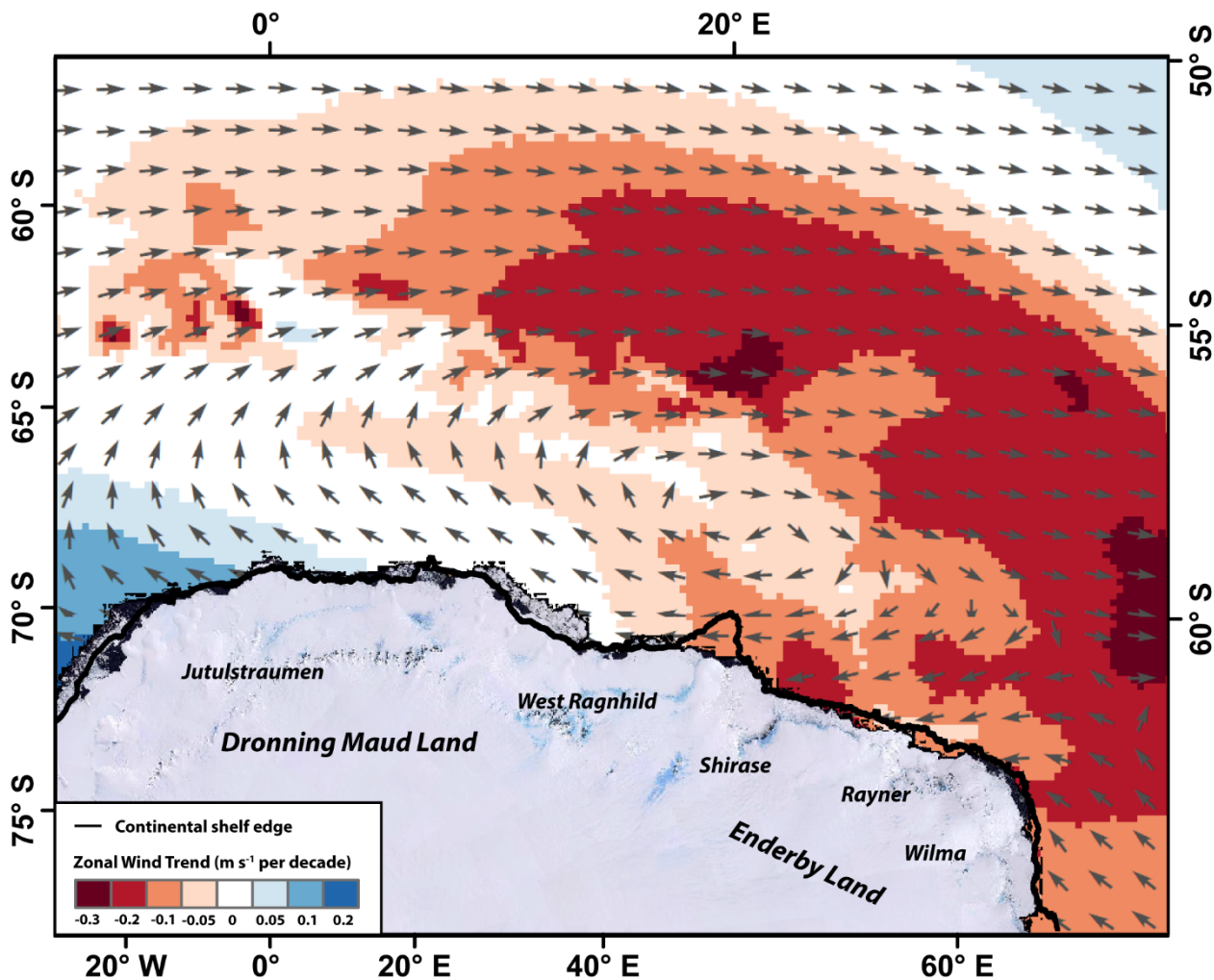


230

231 **Figure 3: a)** Annually averaged ERA5 derived alongshore wind speed from Box A (See Fig. 1) and
 232 plotted as a 5-year rolling mean (black), ice speed at the Shirase Glacier grounding line along T1
 233 (red) and modelled melt rate anomaly of the Shirase ice tongue between 2008 and 2018 plotted as a
 234 1-year rolling mean (blue; Kusahara et al., 2021). Periods of weakening winds cause increased
 235 mCDW transport, increased basal melt and acceleration. Periods of strengthening winds result in
 236 relatively less mCDW transport, decreased basal melt rates and glacier slowdown. Note that

237 alongshore wind speed is plotted with an inverted axis. **b)** Annually averaged ice thickness change at
 238 point IT with respect to 2009/10 (see Fig. 2a) extracted from the Schröder et al. (2019) dataset, where
 239 there are at least 6 data points in the calendar year. The error bars are annually averaged errors. The
 240 background grey points are the raw monthly data points. **c)** Annual averaged precipitation over
 241 Shirase Glacier from the MAR regional climate model (Kittel et al., 2021), uncertainties are not
 242 provided with these data.

243



244

245 **Figure 4:** Linear zonal wind trend 1979-2021 with data smoothed with 60 month moving average
 246 prior to extracting the trend. Negative values indicate a trend for zonal winds in a more easterly
 247 direction and positive values indicate a trend for winds in a more westerly direction. Mean wind
 248 direction (1979-2021) is represented by the grey arrows. Major outlet glaciers have been labelled.

249

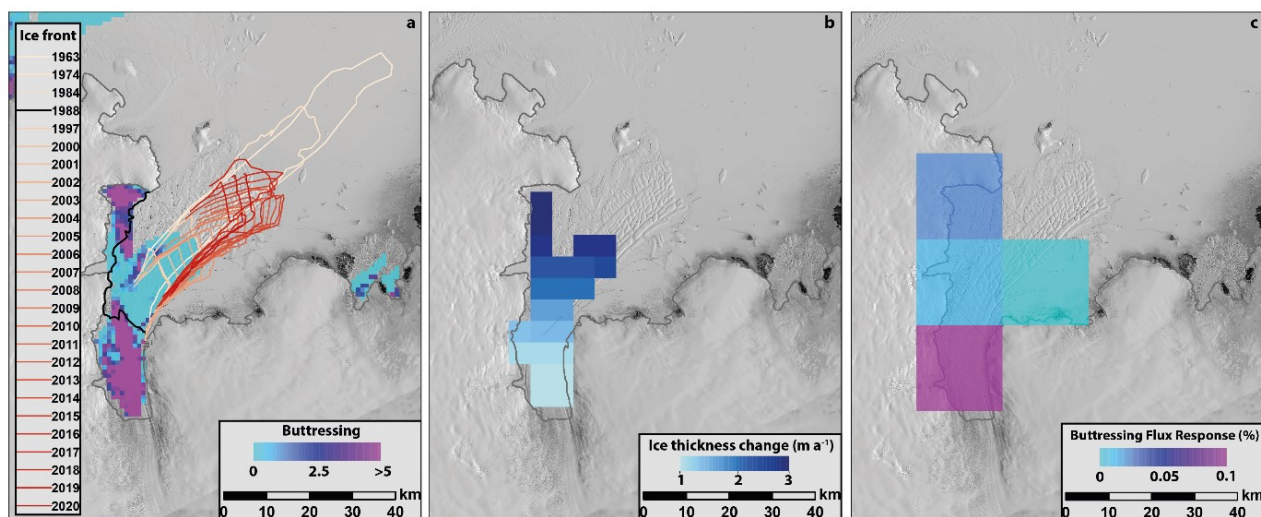
250 4. Discussion

251 4.1 Slowdown and thickening caused by strengthening alongshore winds

252 Calculations indicate that the heavily fractured and unconstrained section of the Shirase ice tongue
 253 conglomerate offers little buttressing force (Fig. 5a; Durrand et al., 2016; Fürst et al., 2016).
 254 Therefore, it is unlikely that any variations in the extent of the Shirase ice tongue have had a direct

255 effect on the ice speed trends we have observed. The only possible exception to this is in 1988 where
256 the ice tongue briefly retreated to the edge of its more confined embayment (Fig. 2a), closer to where
257 the extent of the ice tongue might be expected to exert buttressing and impact on inland flow speed,
258 were it to be removed (Fig. 5a).

259



260

261 **Figure 5: a)** Simulated maximum buttressing potential of the Shirase ice tongue (Durand et al., 2016).
262 Light blues mean the ice is passive, purples mean the floating ice is dynamically important. Note how
263 the ice tongue conglomerate is not important for buttressing, but parts of the inner shelf are important.
264 No dynamically important ice has calved over the past over the past 57 years. **b)** Ice tongue thickness
265 change between 2003 and 2019 showing thickening of the Shirase ice tongue (Smith et al., 2020). **c)**
266 Simulated response of ice flux to thinning of floating ice in each grid cell by 1 m (Reese et al., 2018),
267 the constrained inner tongue near the grounding line is important for buttressing. Note there is no
268 change in ice tongue buttressing in response to observed changes in ice tongue extent, but increased
269 buttressing expected in response to observed ice tongue thickening. Landsat images are courtesy of
270 the U.S. Geological Survey.

271

272 In agreement with previous work, we note that the observed fluctuations in ice tongue extent are
273 correlated with landfast sea-ice conditions in Lützow-Holm Bay (Aoki, 2017). Long periods of ice
274 tongue advance are associated with persistent landfast sea-ice in Lützow-Holm Bay, while ice tongue
275 retreat is associated with landfast sea-ice break-out events removing parts of the ice tongue
276 conglomerate (Aoki et al., 2017). These break-out events have occurred sporadically during the
277 austral summer months (Fig. S1). It is important to note that fast ice only helps control the length of
278 the ice tongue conglomerate (Fig. 1b) and there is no evidence that the fast ice has any major role in
279 providing buttressing for Shirase Glacier. For example, we note that there was no obvious increase in
280 ice speed at the grounding line or over the inner ice tongue in 1988 when the fast ice and ice tongue

281 conglomerate were completely removed from the bay (Fig. 2a, S1), albeit there are large uncertainties
282 in our 1988 ice speed estimate ($\pm 171 \text{ m a}^{-1}$). In addition, Nakamura et al. (2010) recorded only a very
283 modest $20 \pm 30 \text{ m a}^{-1}$ ($0.8 \pm 1.3 \%$) change in ice speed at the grounding line after a partial fast ice
284 break-out event in 1998, and there was also an indistinguishable change in ice speed at the grounding
285 line following a break-out in 2017 (Nakamura et al., 2022).

286 Point IT, 20 km inland of the Shirase Glacier grounding line was thinning at a rate of $-0.27 \pm 0.33 \text{ m}$
287 a^{-1} between 1987 and 1997 (Fig. 3b), a pattern consistent with field observations up to 200 km further
288 inland in the 1960s, 1970s and 1980s (Mae and Naruse, 1978; Naruse, 1979; Nisho et al., 1989; Toh
289 and Shibuya, 1992). However, in ~ 2000 there was a slowdown in Shirase Glacier (Fig. 3a) and this
290 thinning trend reversed to thickening (Fig. 3b). This slowdown and thickening coincides with an
291 increase in alongshore easterly wind speed adjacent to the Shirase coastline (Fig. 3a). The seasonal
292 strengthening in alongshore easterly winds offshore of the Shirase coastline has been observed to
293 deepen the thermocline in Lützow-Holm Bay, limiting the inflow of mCDW onto the continental
294 shelf and reduce basal melt rates (Hirano et al., 2020). We suggest that this same process over annual
295 to decadal timescales has caused the slowdown of Shirase Glacier.

296 Increased alongshore wind speed from ~ 2000 enhanced Ekman convergence at the coast, deepening
297 the thermocline with a short lag and inhibited the inflow of warm mCDW into Lützow-Holm Bay.
298 The subsequent cooling of Lützow-Holm Bay reduced the basal melt rate of the Shirase ice tongue.
299 This reduction in basal melt caused the ice tongue to thicken and is confirmed by ICESat and ICESat-
300 2 observations of the of the Shirase ice tongue that show a mean thickening of 1.87 m yr^{-1} from 2003-
301 2019 (Fig. 5b; Smith et al., 2020). Instantaneous numerical modelling experiments show that ice
302 discharge is sensitive to thickness changes in the inner ice tongue (Reese et al., 2018; Fig. 5c).
303 Therefore, the dynamic thickening of the inner ice tongue would be expected to increase buttressing
304 through time (Fig. 5c) and ultimately drive the overall slowdown in ice speed, grounding line advance
305 and inland thickening that we observe. Importantly, our results show that wind-driven ocean forcing
306 is also contributing to mass gain in the Lützow-Holm Bay. This is likely in addition to surface mass
307 balance processes, as indicated by the widespread inland thickening of the Shirase catchment between
308 2003 and 2019 (Smith et al., 2020). However, there is no evidence of a long-term increase in
309 precipitation at the Shirase catchment (Fig. 3c). Instead the inland thickening is likely a consequence
310 of extreme anomalous snowfall events in 2009 and 2011 (e.g. Boening et al., 2012; Lenaerts et al.,
311 2013).

312 Within the longer-term slowdown of Shirase Glacier between 1973 and 2020 we observe brief periods
313 of acceleration in response to short-lived periods of weakening alongshore winds. For example, both
314 of the accelerations in ice speed from 1997-2000 and 2015-2019 are preceded by brief periods of

315 weakening alongshore winds (Fig. 3a). These periods of weakening alongshore winds cause relatively
316 higher basal melt rates because they raise the thermocline closer to the ocean surface and enable a
317 greater influx of mCDW into Lützow-Holm Bay (Hirano et al., 2020). This is supported by the close
318 relationship between alongshore wind speed and modelled melt rate anomalies (Fig. 3a; Kusahara et
319 al., 2021). Although we do note some slight discrepancies in this relationship, for example between
320 2008 and 2011, changes in melt rates precede changes in winds. This could be related to the relative
321 smoothing of both datasets, with alongshore wind plotted as a 5-year rolling mean and melt rates
322 plotted as a 1-year rolling mean.

323 The interannual variability in ice flow speed at Shirase Glacier in response to wind-forced ocean
324 variability is analogous to other regions of Antarctica where mCDW periodically floods the
325 continental shelf e.g. Pine Island (Christianson et al., 2016), Thwaites (Miles et al., 2020) and Totten
326 glaciers (Greene et al., 2017). The pattern of change at Shirase Glacier is unique, however, in that it
327 is the only outlet glacier in Antarctica with a warm water regime that has been observed to be slowing
328 down and thickening during the 21st century, as opposed to accelerating and thinning (e.g. Mouginit
329 et al., 2014; Greene et al., 2017). As such, our results highlight that this oceanic mode of ice melt is
330 not universally associated with mass loss in Antarctica.

331

332 **4.2 Wider links to climate forcing and future implications**

333 In response to both increased greenhouse gas emissions and ozone depletion (Thompson et al., 2011;
334 Wang et al., 2014; Perren et al., 2020) the band of mid-latitude westerly winds that encircle Antarctica
335 have both strengthened and migrated southwards towards the ice sheet over recent decades
336 (Thompson & Solomon, 2002; Marshall, 2003; Turner, 2005; Bracegirdle et al., 2018). In the
337 Amundsen Sea sector of West Antarctica, this anthropogenically-driven migration has been linked to
338 westerly wind anomalies over the continental shelf (Holland et al., 2019), which have enabled a
339 greater influx of warm mCDW onto the continental shelf and have driven enhanced localized ice
340 sheet mass loss (Thoma et al., 2008). At Shirase Glacier, our observations of strengthening alongshore
341 easterly winds suggest any southward encroachment of the mid-latitude westerlies has yet to impact
342 the Shirase coastline. This may also be the case for parts of the wider Enderby Land coastlines where
343 alongshore easterlies have strengthened along the continental shelf edge (Hazel & Stewart, 2019).
344 However, it remains unknown what effect these strengthening easterly winds may have had on other
345 nearby outlet glaciers (e.g. Rayner and Wilma; Fig. 4), which are yet to be studied in detail. The trend
346 in strengthening alongshore easterlies might also be linked to enhanced katabatic winds as low
347 pressure systems track progressively further south and enhance the pole to coast pressure gradient

348 (Hazel & Stewart, 2019). It is unclear if the enhancement of the pole-to-coast pressure gradient has
349 been influenced by the anthropogenically-driven southerly migration of the mid-latitude westerlies,
350 or if it has been caused by inherent natural decadal variability within the system.

351 Over the course of the 21st century, the southerly migration of the mid-latitude westerlies is projected
352 to continue in a warming climate (Yin, 2005; Perren et al., 2020). Along the Shirase coastline, this
353 continued southerly migration may ultimately result in a similar situation to the Amundsen Sea, such
354 that westerly wind anomalies offshore would result in enhanced mCDW transport into Lützow-Holm
355 Bay and cause mass loss. Alternatively, the westerly winds may never migrate close enough to the
356 Shirase coastline to impact alongshore winds, and instead, alongshore winds may continue to
357 strengthen as the pole to coast pressure gradient increases. This would result in further cooling of
358 Lützow-Holm Bay and ice tongue thickening, and further mass gain. In a wider context, an improved
359 understanding of the potential changes in ocean forcing in response to broader atmospheric patterns
360 expected over the coming decades is needed in the Enderby and Dronning Maud Land sectors.

361

362 **5. Conclusion**

363 Our observations of Shirase Glacier are a rare example of a glacier reversing a trend of mass loss
364 from at least the 1970s-1990s to mass gain over the last two decades. As far as we are aware this is
365 the only major fast flowing Antarctic outler glacier to display this pattern of behaviour. This reversal
366 has been driven by a slowdown of the Shirase Glacier upstream of the grounding line in response to
367 strengthening alongshore easterly winds that have limited the inflow of warm mCDW into Lützow-
368 Holm Bay, reduced basal melt rates, and caused its ice tongue to dynamically thicken. Should this
369 strengthening of alongshore easterly winds continue into the future, the Shirase catchment will
370 continue to experience a positive mass balance due to both the slow-down in ice discharge, and to the
371 predicted increase in precipitation in response to atmospheric warming (e.g. Ligtenberg et al., 2013;
372 Kittel et al., 2021). Our results highlight the need for a greater consideration of the potential role of
373 ocean forcing in both the current and future mass balance of the wider Enderby and Dronning Maud
374 Land regions.

375

376 **Data Availability**

377 Landsat and ARGON imagery was provided free of charge by the US Geological Survey Earth
378 Resources Observation Science Center (<https://earthexplorer.usgs.gov/>). For the MODIS imagery we
379 also acknowledge the use of imagery from the NASA Worldview application

380 (<https://worldview.earthdata.nasa.gov>), part of the NASA Earth Observing System Data and
381 Information System (EOSDIS). Cosi-corr is an ENVI plug-in and can be downloaded from
382 http://www.tectonics.caltech.edu/slip_history/spot_coseis/download_software.html. The ITS_LIVE
383 velocity products are available from <https://doi.org/10.5067/IMR9D3PEI28U>. GoLIVE velocity
384 products are available from <http://dx.doi.org/10.7265/N5ZP442B>. ERA5 data is available from
385 <https://doi.org/10.24381/cds.adbb2d47>. Wind data from Syowa station is available via the SCAR
386 READER at <http://dx.doi.org/10.5285/569d53fb-9b90-47a6-b3ca-26306e696706>. The MOA
387 grounding line product is available at <https://doi.org/10.7265/N5KP8037>. BedMachine is available at
388 <https://doi.org/10.5067/E1QL9HFQ7A8M>. The ice shelf thickness change dataset from Smith et al.
389 (2020) is available at <http://hdl.handle.net/1773/45388>. REMA DEM strips are available at
390 <https://www.pgc.umn.edu/data/rema/>. Lützw-Holm Bay bathymetry is available at
391 <https://doi.org/10.17632/z6w4xd6s3s.1>. The RAMP mosaic is available at <https://doi.org/10.5067/8AF4ZRPULS4H>. Ice shelf extent buttressing dataset from Durand et al., 2016 is available at
392 <https://doi.org/10.5067/FWHORAYVZCE7>. SPIRIT DEM's are available from
393 <https://theia.cnes.fr/atdistrib/rocket/#/search?collection=spirit>. MAR precipitation data is available
394 from <https://doi.org/10.5281/zenodo.4459259>.

396

397 **Acknowledgements**

398 This research has been supported by a UK Natural Environment Research Council (NERC) grant
399 (NE/R000824/1). BM was also supported by a Leverhulme Early Career Fellowship (ECF-2021-
400 484). Hersbach, H. et al.'s (2018) dataset was downloaded from the Copernicus Climate Change
401 Service (C3S) Climate Data Store. We acknowledge the DEMs provided by the Byrd Polar and
402 Climate Research Center and the Polar Geospatial Center under NSF-OPP awards 1543501, 1810976,
403 1542736, 1559691, 1043681, 1541332, 0753663, 1548562, 1238993 and NASA award
404 NNX10AN61G. Computer time provided through a Blue Waters Innovation Initiative. DEMs
405 produced using data from Maxar. We thank Ronja Reese for providing the ice flux buttressing
406 response dataset. We would like to thank two anonymous reviewers, along with the editor Etienne
407 Berthier, for providing constructive comments which led to the improvement of this paper.

408

409 **Author contributions:** All authors contributed to the design of the study. BWJM collected and
410 analysed the remote sensing data and led the manuscript writing with input from all authors.

411

412 **Competing interests:** The authors declare no competing interests

413

414 **References**

- 415 Aoki, S., Ozawa, T. & Doi, K.: GPS observation of the sea level variation in Lützow-Holm Bay,
416 Antarctica. *Geophysical Research Letters*, 27(15), 2285–2288.
417 <https://doi.org/10.1029/1999GL011304>, 2000.
- 418 Aoki, S.: Breakup of land-fast sea ice in Lützow-Holm Bay, East Antarctica, and its teleconnection
419 to tropical Pacific sea surface temperatures. *Geophysical Research Letters*, 44(7), 3219–3227.
420 <https://doi.org/10.1002/2017GL072835>, 2017.
- 421 Aoyama, Y., Doi, K., Shibuya, K., Ohta, H., & Tsuwa, I.: Near real-time monitoring of flow
422 velocity and direction in the floating ice tongue of the Shirase Glacier using low-cost GPS
423 buoys. *Earth, Planets and Space*, 65(2), 103–108. <https://doi.org/10.5047/EPS.2012.06.011>,
424 2013.
- 425 Boening, C., Lebrock, M., Landerer, F., & Stephens, G.: Snowfall-driven mass change on the East
426 Antarctic ice sheet. *Geophysical Research Letters*, 39(21).
427 <https://doi.org/10.1029/2012GL053316>, 2012.
- 428 Bracegirdle, T. J., Hyder, P., & Holmes, C. R.: CMIP5 Diversity in Southern Westerly Jet
429 Projections Related to Historical Sea Ice Area: Strong Link to Strengthening and Weak Link to
430 Shift. *Journal of Climate*, 31(1), 195–211. <https://doi.org/10.1175/JCLI-D-17-0320.1>, 2018.
- 431 Brunt, K. M., Fricker, H. A., Padman, L., Scambos, T. A., & O’Neel, S.: Mapping the grounding
432 zone of the Ross Ice Shelf, Antarctica, using ICESat laser altimetry. *Annals of Glaciology*,
433 51(55), 71–79. <https://doi.org/10.3189/172756410791392790>, 2010.
- 434 Christianson, K., Bushuk, M., Dutrieux, P., Parizek, B. R., Joughin, I. R., Alley, R. B., et al.:
435 Sensitivity of Pine Island Glacier to observed ocean forcing. *Geophysical Research Letters*,
436 43(20), 10,817–10,825. <https://doi.org/10.1002/2016GL070500>, 2016.
- 437 Cook, A. J., Holland, P. R., Meredith, M. P., Murray, T., Luckman, A., & Vaughan, D. G.: Ocean
438 forcing of glacier retreat in the western Antarctic Peninsula. *Science*, 353(6296), 283–286,
439 2016.
- 440 Durand, G., F. Gillet-Chaulet, O. Gagliardini, and J. J. Fürst.: SUMER Antarctic Ice-shelf
441 Buttressing, Version 1. Boulder, Colorado USA. NASA National Snow and Ice Data Center
442 Distributed Active Archive Center. <https://doi.org/10.5067/FWHORAYVZCE7>, 2016
- 443 Fahnestock, M., Scambos, T., Moon, T., Gardner, A., Haran, T., & Klinger, M.: Rapid large-area
444 mapping of ice flow using Landsat 8. *Remote Sensing of Environment*, 185, 84–94.
445 <https://doi.org/10.1016/J.RSE.2015.11.023>, 2016.
- 446 Fricker, H. A., Coleman, R., Padman, L., Scambos, T. A., Bohlander, J., & Brunt, K. M.: Mapping
447 the grounding zone of the Amery Ice Shelf, East Antarctica using InSAR, MODIS and ICESat.
448 *Antarctic Science*, 21(5), 515–532. <https://doi.org/10.1017/S095410200999023X>, 2009.
- 449 Fürst, J. J., Durand, G., Gillet-Chaulet, F., Tavard, L., Rankl, M., Braun, M., & Gagliardini, O.: The
450 safety band of Antarctic ice shelves. *Nature Climate Change*, 6(5), 479–482.
451 <https://doi.org/10.1038/nclimate2912>, 2016.
- 452 Gardner, A., Fahnestock, M., & Scambos, T. A.: ITS_LIVE Regional Glacier and Ice Sheet Surface
453 Velocities. <https://doi.org/doi:10.5067/6II6VW8LLWJ7>, 2020.

- 454 Gardner, A. S., Moholdt, G., Scambos, T., Fahnestock, M., Ligtenberg, S., van den Broeke M., &
455 Nilsson, J.: Increased West Antarctic and unchanged East Antarctic ice discharge over the last
456 7 years. *Cryosphere*, 12(2), 521–547. <https://doi.org/10.5194/TC-12-521-2018>, 2018.
- 457 Greene, C. A., Blankenship, D. D., Gwyther, D. E., Silvano, A., & van Wijk, E.: Wind causes
458 Totten Ice Shelf melt and acceleration. *Science Advances*, 3(11), e1701681–e1701681.
459 <https://doi.org/10.1126/sciadv.1701681>, 2017.
- 460 Haran, T., J. Bohlander, T. Scambos, T. Painter, and M. Fahnestock.: MODIS Mosaic of Antarctica
461 2008-2009 (MOA2009) Image Map, Version 2. Boulder, Colorado USA. NASA National
462 Snow and Ice Data Center Distributed Active Archive Center. doi:
463 <https://doi.org/10.5067/4ZL43A4619AF>, 2019
- 464 Hazel, J. E., & Stewart, A. L.: Are the Near-Antarctic Easterly Winds Weakening in Response to
465 Enhancement of the Southern Annular Mode? *Source: Journal of Climate*, 32(6), 1895–1918.
466 <https://doi.org/10.2307/26663209>, 2019.
- 467 Hersbach, H., Bell, B., Berrisford, P., Hirahara, S., Horányi, A., Muñoz-Sabater, J., et al.: The
468 ERA5 global reanalysis. *Quarterly Journal of the Royal Meteorological Society*, 146(730),
469 1999–2049. <https://doi.org/10.1002/QJ.3803>, 2020.
- 470 Heid, T., & Kääb, A.: Evaluation of existing image matching methods for deriving glacier surface
471 displacements globally from optical satellite imagery. *Remote Sensing of Environment*, 118,
472 339–355. <https://doi.org/10.1016/J.RSE.2011.11.024>, 2012.
- 473 Hirano, D., Tamura, T., Kusahara, K., Ohshima, K. I., Nicholls, K. W., Ushio, S., et al.: Strong ice-
474 ocean interaction beneath Shirase Glacier Tongue in East Antarctica. *Nature Communications*
475 2020 11:1, 11(1), 1–12. <https://doi.org/10.1038/s41467-020-17527-4>, 2020.
- 476 Holland, P. R., Bracegirdle, T. J., Dutrieux, P., Jenkins, A., & Steig, E. J. (2019). West Antarctic ice
477 loss influenced by internal climate variability and anthropogenic forcing. *Nature Geoscience*
478 2019 12:9, 12(9), 718–724. <https://doi.org/10.1038/s41561-019-0420-9>
- 479 Howat, I. M., Porter, C., Smith, B. E., Noh, M. J., & Morin, P.: The reference elevation model of
480 antarctica. *Cryosphere*, 13(2), 665–674. <https://doi.org/10.5194/TC-13-665-2019>, 2019.
- 481 Jacobs, S. S., Helmer, H. H., Doake, C. S. M., Jenkins, A., & Frolich, R. M.: Melting of ice shelves
482 and the mass balance of Antarctica. *Journal of Glaciology*, 38(130), 375–387.
483 <https://doi.org/10.3189/S0022143000002252>, 1992.
- 484 Jenkins, A., Shoosmith, D., Dutrieux, P., Jacobs, S., Kim, T. W., Lee, S. H., et al.: West Antarctic
485 Ice Sheet retreat in the Amundsen Sea driven by decadal oceanic variability, 11(10), 733–738.
486 <https://doi.org/10.1038/s41561-018-0207-4>, 2018.
- 487 Jezek, K. C., J. C. Curlander, F. Carsey, C. Wales, and R. G. Barry.: RAMP AMM-1 SAR Image
488 Mosaic of Antarctica, Version 2. Boulder, Colorado USA. NASA National Snow and Ice Data
489 Center Distributed Active Archive Center. <https://doi.org/10.5067/8AF4ZRPULS4H>, 2013.
- 490 Kameda, T., Nakawo, M., Mae, S., Watanabe, O., & Naruse, R.: Thinning of the Ice Sheet
491 Estimated from Total Gas Content of Ice Cores in Mizuho Plateau, East Antarctica. *Annals of*
492 *Glaciology*, 14, 131–135. <https://doi.org/10.3189/S0260305500008429>, 1990.

- 493 Kittel, C., Amory, C., Agosta, C., Jourdain, N. C., Hofer, S., Delhasse, A., et al.: Diverging future
494 surface mass balance between the Antarctic ice shelves and grounded ice sheet. *Cryosphere*,
495 *15*(3), 1215–1236. <https://doi.org/10.5194/TC-15-1215-2021>, 2021.
- 496 Konrad, H., Shepherd, A., Gilbert, L., Hogg, A. E., McMillan, M., Muir, A., & Slater, T.: Net
497 retreat of Antarctic glacier grounding lines. *Nature Geoscience*, *11*(4), 258–262.
498 <https://doi.org/10.1038/s41561-018-0082-z>, 2018.
- 499 Korona, J., Berthier, E., Bernard, M., Rémy, F and Thouvenot, E.: ISPRS Journal of Photogrammetry
500 and Remote Sensing SPIRIT. SPOT 5 stereoscopic survey of Polar Ice: reference images and
501 topographies during the fourth International Polar Year (2007–2009). *ISPRS Journal of*
502 *Photogrammetry and Remote Sensing* *64*(2), 204–212. doi: 10.1016/j.isprsjprs.2008.10.005,
503 2009.
- 504 Kusahara, K., Hirano, D., Fujii, M., D. Fraser, A., & Tamura, T.: Modeling intensive ocean-
505 cryosphere interactions in Lützow-Holm Bay, East Antarctica. *Cryosphere*, *15*(4), 1697–1717.
506 <https://doi.org/10.5194/TC-15-1697-2021>, 2021
- 507 Lenaerts, J. T. M., van Meijgaard, E., van den Broeke, M. R., Ligtenberg, S. R. M., Horwath, M., &
508 Isaksson, E.: Recent snowfall anomalies in Dronning Maud Land, East Antarctica, in a
509 historical and future climate perspective. *Geophysical Research Letters*, *40*(11), 2684–2688.
510 <https://doi.org/10.1002/GRL.50559>, 2013.
- 511 Leprince, S., Ayoub, F., Klinger, Y., & Avouac, J.-P.: *Co-Registration of Optically Sensed Images*
512 *and Correlation (COSI-Corr): an Operational Methodology for Ground Deformation*
513 *Measurements*. Igarss: 2007 Ieee International Geoscience and Remote Sensing Symposium,
514 1–12,1943–1946. <https://doi.org/10.1109/Igarss.2007.4423207>, 2007.
- 515 Ligtenberg, S. R. M., van de Berg, W. J., van den Broeke, M. R., Rae, J. G. L., & van Meijgaard,
516 E.: Future surface mass balance of the Antarctic ice sheet and its influence on sea level change,
517 simulated by a regional atmospheric climate model. *Climate Dynamics*, *41*(3–4), 867–884.
518 <https://doi.org/10.1007/S00382-013-1749-1>, 2013.
- 519 Mae, S., & Naruse, R. : Possible causes of ice sheet thinning in the Mizuho Plateau. *Nature* *1978*
520 *273:5660*, *273*(5660), 291–292. <https://doi.org/10.1038/273291a0>, 1978.
- 521 Marshall, G.: Trends in the Southern Annular Mode from observations and reanalyses. *J. Clim.*, *16*,
522 4134–4143, 2003.
- 523 Miles, B. W. J. J., Stokes, C. R., Jenkins, A., Jordan, J. R., Jamieson, S. S. R. R., & Gudmundsson,
524 G. H.: Intermittent structural weakening and acceleration of the Thwaites Glacier Tongue
525 between 2000 and 2018. *Journal of Glaciology*, 1–11. <https://doi.org/10.1017/jog.2020.20>,
526 2020.
- 527 Moriwaki, K., & Yoshida, Y.: Submarine topography of Lützow-Holm Bay, Antarctica. *Mem. Natl.*
528 *Inst. Polar Res.*, *28*, 247–258, 1983.
- 529 Morlighem, M.: MEaSURES BedMachine Antarctica, Version 2. Boulder, Colorado USA. NASA
530 National Snow and Ice Data Center Distributed Active Archive Center. doi:
531 <https://doi.org/10.5067/E1QL9HFQ7A8M>, 2020.
- 532 Morlighem, M., Rignot, E., Binder, T., Blankenship, D., Drews, R., Eagles, G., et al.: Deep glacial
533 troughs and stabilizing ridges unveiled beneath the margins of the Antarctic ice sheet. *Nature*
534 *Geoscience*, *13*(2), 132–137. <https://doi.org/10.1038/s41561-019-0510-8>, 2020.

- 535 Mougnot, J., Rignot, E., & Scheuchl, B.: Sustained increase in ice discharge from the Amundsen
536 Sea Embayment, West Antarctica, from 1973 to 2013. *Geophysical Research Letters*, 41(5),
537 1576–1584. <https://doi.org/10.1002/2013GL059069>, 2014.
- 538 Nakamura, K., Doi, K., & Shibuya, K.: Estimation of seasonal changes in the flow of Shirase
539 Glacier using JERS-1/SAR image correlation. *Polar Science*, 1(2–4), 73–83.
540 <https://doi.org/10.1016/J.POLAR.2007.09.002>, 2007.
- 541 Nakamura, K., Doi, K., & Shibuya, K.: Fluctuations in the flow velocity of the Antarctic Shirase
542 Glacier over an 11-year period. *Polar Science*, 4(3), 443–455.
543 <https://doi.org/10.1016/J.POLAR.2010.04.010>, 2010.
- 544 Nakamura, K., Aoki, S., Yamanokuchi, T., and Tamura, T.: Interactive movements of outlet glacier
545 tongue and landfast sea ice in Lützow-Holm Bay, East Antarctica, detected by ALOS-
546 2/PALSAR-2 imagery. *Science of Remote Sensing*, 6, 100064.
547 <https://doi.org/10.1016/j.srs.2022.100064>, 2022.
- 548 Naruse, R.: Thinning of the Ice Sheet in Mizuho Plateau, East Antarctica. *Journal of Glaciology*,
549 24(90), 45–52. <https://doi.org/10.3189/S0022143000014635>, 1979.
- 550 Nishio, F., Mae, S., Ohmae, H., Takahashi, S., Nakawo, M., & Kawada, K.: Dynamical behaviour
551 of the ice sheet in Mizuho Plateau, East Antarctica. *Proc. NIPR Symp. Polar Meteorol.*
552 *Glaciol.*, 2, 97–104, 1989.
- 553 Ohshima, K. I., Takizawa, T., Ushio, S., & Kawamura, T.: Seasonal variations of the Antarctic
554 coastal ocean in the vicinity of Lützow-Holm Bay. *Journal of Geophysical Research C:*
555 *Oceans*, 101(C9), 20617–20628. <https://doi.org/10.1029/96JC01752>, 1996.
- 556 Pattyn, F., & Derauw, D.: Ice-dynamic conditions of Shirase Glacier, Antarctica, inferred from ERS
557 SAR interferometry. *Journal of Glaciology*, 48(163), 559–565.
558 <https://doi.org/10.3189/172756502781831115>, 2002.
- 559 Pattyn, F., & Naruse, R.: The nature of complex ice flow in Shirase Glacier catchment, East
560 Antarctica. *Journal of Glaciology*, 49(166), 429–436.
561 <https://doi.org/10.3189/172756503781830610>, 2003.
- 562 Perren, B. B., Hodgson, D. A., Roberts, S. J., Sime, L., van Nieuwenhuyze, W., Verleyen, E., &
563 Vyverman, W.: Southward migration of the Southern Hemisphere westerly winds corresponds
564 with warming climate over centennial timescales. *Communications Earth & Environment* 2020
565 1:1, 1(1), 1–8. <https://doi.org/10.1038/s43247-020-00059-6>, 2020.
- 566 Reese, R., Gudmundsson, G. H., Levermann, A., & Winkelmann, R.: The far reach of ice-shelf
567 thinning in Antarctica. *Nature Climate Change*, 8(1), 53– 57. <https://doi.org/10.1038/s41558-017-0020-x>, 2018.
- 569 Rignot, E., Mougnot, J., Scheuchl, B., van den Broeke, M., van Wessem, M. J., & Morlighem, M.:
570 Four decades of Antarctic ice sheet mass balance from 1979–2017. *Proceedings of the*
571 *National Academy of Sciences of the United States of America*. National Academy of Sciences.
572 <https://doi.org/10.1073/pnas.1812883116>, 2019.
- 573 Rintoul, S. R., Silvano, A., Pena-Molino, B., van Wijk, E., Rosenberg, M., Greenbaum, J. S., &
574 Blankenship, D. D.: Ocean heat drives rapid basal melt of the Totten ice shelf. *Science*
575 *Advances*, 2(12). <https://doi.org/10.1126/sciadv.1601610>, 2016.

- 576 Scambos, T., Fahnestock, M., Moon, T., Gardner, A., & Klinger, M.: Global Land Ice Velocity
577 Extraction from Landsat 8 (GoLIVE). Boulder, Colorado USA. NSIDC: National Snow and
578 Ice Data Center, 2016.
- 579 Scambos, T. A., Haran, T. M., Fahnestock, M. A., Painter, T. H., & Bohlander, J.: MODIS-based
580 Mosaic of Antarctica (MOA) data sets: Continent-wide surface morphology and snow grain
581 size. *Remote Sensing of Environment*, 111(2), 242–257.
582 <https://doi.org/10.1016/J.RSE.2006.12.020>, 2007.
- 583 Scherler, D., Leprince, S., & Strecker, M. R.: Glacier-surface velocities in alpine terrain from
584 optical satellite imagery—Accuracy improvement and quality assessment. *Remote Sensing of*
585 *Environment*, 112(10), 3806–3819. <https://doi.org/10.1016/J.RSE.2008.05.018>, 2008.
- 586 Schröder, L., Horwath, M., Dietrich, R., & Helm, V.: Four decades of surface elevation change of
587 the Antarctic Ice Sheet from multi-mission satellite altimetry. *The Cryosphere*, 13, 427–449,
588 <https://doi.org/10.5194/tc-13-427-2019>, 2019.
- 589 Smith, B., Fricker, H. A., Gardner, A. S., Medley, B., Nilsson, J., Paolo, F. S., Nicholas Holschuh,
590 et al.: Pervasive ice sheet mass loss reflects competing ocean and atmosphere processes.
591 *Science*, 368(6496), 1239–1242, 2020.
- 592 Sproson, A. D., Takano, Y., Miyairi, Y., Aze, T., Matsuzaki, H., Ohkouchi, N., & Yokoyama, Y.:
593 Beryllium isotopes in sediments from Lake Maruwan Oike and Lake Skallen, East Antarctica,
594 reveal substantial glacial discharge during the late Holocene. *Quaternary Science Reviews*,
595 256, 106841. <https://doi.org/10.1016/J.QUASCIREV.2021.106841>, 2021.
- 596 Stokes, C.R., Abram, N.J., Bentley, M.J. et al.: Response of the East Antarctic Ice Sheet to past and
597 future climate change. *Nature* 608, 275–286, <https://doi.org/10.1038/s41586-022-04946-0>,
598 2022
- 599 Thoma, M., Jenkins, A., Holland, D., & Jacobs, S.: Modelling Circumpolar Deep Water intrusions
600 on the Amundsen Sea continental shelf, Antarctica. *Geophysical Research Letters*, 35(18).
601 <https://doi.org/10.1029/2008GL034939>, 2008.
- 602 Thompson, D. W. J., & Solomon, S.: Interpretation of recent Southern Hemisphere climate change.
603 *Science*, 296(5569), 895–899. <https://doi.org/10.1126/science.1069270>, 2002.
- 604 Thompson, D. W. J., Solomon, S., Kushner, P. J., England, M. H., Grise, K. M., & Karoly, D. J.:
605 Signatures of the Antarctic ozone hole in Southern Hemisphere surface climate change. *Nature*
606 *Geoscience* 2011 4:11, 4(11), 741–749. <https://doi.org/10.1038/ngeo1296>, 2011.
- 607 Toh, H. and Shibuya, K.: Thinning rate of ice sheet on Mizuho Plateau, East Antarctica, determined
608 by GPS differential positioning. In Yoshida, Y., Kaminuma, K. and Shiraishi, K., eds. Recent
609 progress in Antarctic earth sciences. Tokyo, Terra Scientific Publishing Co., 579–583, 1992.
- 610 Turner, J., Colwell, S. R., Marshall, G. J., Lachlan-Cope, T. A., Carleton, A. M., Jones, P. D.,
611 Lagon, V., Reid, P. A., & Iagovkina, S.: The SCAR READER Project: Toward a High-Quality
612 Database of Mean Antarctic Meteorological Observations, *Journal of Climate*, 17(14), 2890–
613 2898, 2004.
- 614 Turner, J.: Antarctic climate change during the last 50 years. *Int. J. Climatol.*, 25, 279–294, 2005
- 615 Wang, G., Cai, W., & Purich, A.: Trends in Southern Hemisphere wind-driven circulation in
616 CMIP5 models over the 21st century: Ozone recovery versus greenhouse forcing. *Journal of*

617 *Geophysical Research: Oceans*, 119(5), 2974–2986. <https://doi.org/10.1002/2013JC009589>,
618 2014.

619 Yin, J. H.: A consistent poleward shift of the storm tracks in simulations of 21st century climate.
620 *Geophys. Res. Lett.*, 32(18), L18701. <https://doi.org/10.1029/2005gl023684>, 2005.

621